

1 **Assimilation of SMAP and ASCAT Soil Moisture Retrievals into the**
2 **JULES Land Surface Model Using the Local Ensemble Transform**
3 **Kalman Filter**

4
5 Eunkyo Seo¹, Myong-In Lee^{1*}, Rolf H. Reichle²

6
7 ¹School of Urban and Environmental Engineering, Ulsan National Institute of Science and
8 Technology, Ulsan, Republic of Korea

9 ²Global Modeling and Assimilation Office, NASA Goddard Spaceflight Center, Greenbelt,
10 MD, United States

11
12 24 November 2020

13
14 Revised DRAFT

15 Submitted to Remote Sensing of Environment

16 Eunkyo Seo is currently affiliated in ‘*Center for Ocean-Land-Atmosphere Studies, George*
17 *Mason University, Fairfax, Virginia, United States*’

18 _____
19 *Corresponding author: Prof. Myong-In Lee, School of Urban and Environmental Engineering,
20 Ulsan National Institute of Science and Technology, 50 UNIST-gil, Ulsan 44919, Republic of
21 Korea (milee@unist.ac.kr)

22

Abstract

23 A land data assimilation system is developed to merge satellite soil moisture retrievals into the Joint
24 U.K. Land Environment Simulator (JULES) land surface model (LSM) using the Local Ensemble
25 Transform Kalman Filter (LETKF). The system assimilates microwave soil moisture retrievals from
26 the Soil Moisture Active Passive (SMAP) radiometer and the Advanced Scatterometer (ASCAT) after
27 bias correction based on cumulative distribution function fitting. The soil moisture assimilation
28 estimates are evaluated with ground-based soil moisture measurements over the continental U.S. for
29 five consecutive warm seasons (May–September of 2015–2019). The result shows that both SMAP and
30 ASCAT retrievals improve the accuracy of soil moisture estimates. Especially, the SMAP single-sensor
31 assimilation experiment shows the best performance with the increase of temporal anomaly correlation
32 by $\Delta R \sim 0.05$ for surface soil moisture and $\Delta R \sim 0.03$ for root-zone soil moisture compared with the
33 LSM simulation without satellite data assimilation. SMAP assimilation is more skillful than ASCAT
34 assimilation primarily because of the greater skill of the assimilated SMAP retrievals compared to the
35 ASCAT retrievals. The skill improvement also depends significantly on the region; the higher skill
36 improvement in the western U.S. compared to the eastern U.S. is explained by the Kalman gain in the
37 two experiments. Additionally, the regional skill differences in the single-sensor assimilation
38 experiments are attributed to the number of assimilated observations. Finally, the soil moisture
39 assimilation estimates provide more realistic land surface information than model-only simulations for
40 the 2015 and the 2016 western U.S. droughts, suggesting the advantage of using satellite soil moisture
41 retrievals in the current drought monitoring system.

42

43 **Keywords:** Soil moisture assimilation; LETKF; JULES LSM; SMAP; ASCAT

44

45 **1. Introduction**

46 Land surface conditions play an important role in drought development, runoff generation, and
47 many other processes related to the land-atmosphere exchange of energy and water (Bateni and
48 Entekhabi 2012; Seneviratne et al., 2010; Seneviratne et al., 2006). In particular, soil moisture states
49 have a memory operating at 1–2 month (i.e., subseasonal) time scales (Koster et al., 2011; Seo et al.,
50 2019; Seo et al., 2020). In future climate scenarios, the role of the land surface may increase with
51 enhanced land-atmosphere coupling, and an expansion of the coupling area may increase the potential
52 risk of severe droughts and heat waves (Dirmeyer et al., 2013). Soil moisture conditions are typically
53 inferred from (1) ground-based observations, (2) remote-sensing retrievals from active and passive
54 microwave satellite sensors, or (3) land surface model (LSM) simulations forced with surface
55 meteorological data from observations or atmospheric analysis estimates. In situ measurements provide
56 the most reliable land information of the surface and sub-subsurface layers at the measurement location
57 but have limitations in terms of spatial and temporal resolution and coverage. Satellite remote sensing
58 provides only surface soil moisture conditions due to the limitation in penetration depth. LSM
59 simulations provide complete spatio-temporal coverage but contain potentially large uncertainties in
60 the model physical parameterization and the surface meteorological forcing variables.

61 Space-borne microwave instruments can be used to retrieve surface soil moisture by measuring
62 soil dielectric properties. Past and current microwave instruments include the X-band (10.7 GHz) and
63 C-band (6.9 GHz) channels of the passive Advanced Microwave Scanning Radiometer (AMSR-E; Owe
64 et al., 2008; Owe et al., 2001) and its successor (AMSR2; Parinussa et al., 2015), the X-band (10.65
65 GHz) passive Tropical Rainfall Measuring Mission (TRMM) Microwave Imager (TMI; Gao et al.,
66 2006), the C-band (6.63 GHz) passive Scanning Multichannel Microwave Radiometer (SMMR; De Jeu
67 2003), the C-band (~5.4 GHz) multi-angular Sentinel-1 Synthetic Aperture Radar (SAR) data (Torres
68 et al., 2012), and the C-band (5.3 GHz) active (radar) microwave Advanced Scatterometer (ASCAT;
69 Wagner et al., 2013). The Soil Moisture and Ocean Salinity (SMOS; Kerr et al., 2010) and Soil Moisture
70 Active Passive (SMAP; Entekhabi et al., 2010a) sensors measure passive microwaves at L-band (1.4

71 GHz) frequencies and are specifically designed to retrieve surface soil moisture. The typical soil
72 penetration depth ranges from ~1-2 cm for X- and C-band retrievals to ~5 cm for L-band retrievals. The
73 spatial (horizontal) resolution is ~20 km for X- and C-band retrievals and ~40 km for L-band retrievals.

74 Land data assimilation can be used to combine the soil moisture information from diverse
75 satellite observations with the advantages of LSMs (Reichle 2008). Most previous studies on land data
76 assimilation adopted simplified or ensemble-based filtering methods such as the Extended Kalman
77 Filter (EKF) or the Ensemble Kalman Filter (EnKF) rather than variational assimilation approaches,
78 which require an adjoint of the land surface model that is difficult to derive (Lahoz and De Lannoy
79 2014; Reichle et al., 2001). In ensemble-based methods, the background error covariance is diagnosed
80 from the ensemble of (nonlinear) land model simulations. The NASA Goddard Earth Observing System
81 (GEOS) land data assimilation system adopted the EnKF to constrain modeled land surface variables
82 using satellite measurements such as soil moisture (Reichle et al., 2008; Reichle et al., 2002a; Reichle
83 et al., 2002b), land surface temperature (Reichle et al., 2010), snow (De Lannoy et al., 2010), and
84 terrestrial water storage (Forman et al., 2012). The European Centre for Medium-Range Weather
85 Forecasts numerical weather prediction system relies on an EKF-based land surface data assimilation
86 system that combines conventional near-surface observations (two-meter air temperature and relative
87 humidity) with ASCAT surface soil moisture retrievals (Albergel et al., 2012; De Rosnay et al., 2013).

88 Several previous studies perform soil moisture assimilation experiments and evaluate the
89 resulting soil moisture estimates against in situ observations. For example, Liu et al., (2011)
90 demonstrated that assimilating AMSR-E soil moisture retrievals increases soil moisture skill compared
91 to an LSM simulation without data assimilation (often referred to as the “open loop”) and Albergel et
92 al., (2012) showed a benefit of assimilating ASCAT satellite for improved soil moisture analysis.
93 Assimilating ASCAT and AMSR-E soil moisture retrievals yields comparable skill improvements, and
94 assimilating both data sets consistently matched or exceeded the best results from the single-sensor
95 assimilation experiments (Draper et al., 2012). De Lannoy and Reichle (2016) found that the
96 assimilation of SMOS soil moisture retrievals or brightness temperatures results in improved soil

97 moisture estimates over North America and Ridler et al., (2014) also addressed the improvement in
98 Western Denmark. Moreover, Pan et al., (2016) suggested that SMAP provides significant added value
99 for data assimilation. Similarly, Lievens et al., (2017) demonstrated soil moisture skill improvements
100 through SMAP and Sentinel-1 data assimilation. Finally, the global SMAP Level-4 Surface and Root-
101 zone Soil Moisture (L4_SM) product, which has been produced operationally by assimilating SMAP
102 L-band brightness temperature observations into the NASA Catchment LSM at 9-km resolution with
103 ~3-day latency since 2015 (Reichle et al., 2017a; Reichle et al., 2017b), has significantly higher skill
104 than model-only soil moisture estimates (Reichle et al., 2019).

105 Based on the aforementioned studies, SMAP satellite retrievals have a strong sensitivity to
106 soil moisture in a slightly deeper surface layer and perform better in satellite data assimilation than other
107 satellite soil moisture retrievals (Al-Yaari et al., 2019). On the other hand, ASCAT satellite retrievals
108 have been available from the Meteorological Operational Satellite (METOP)-A launched in 2006, the
109 METOP-B in 2012, and the most recently launched METOP-C in 2018, which provide the data with
110 wide spatial coverage for global analysis as well as long-term data useful for climate reanalysis. Due to
111 these advantages, SMAP and ASCAT have been widely used by many U.S. and European institutes in
112 operation and research for the satellite soil moisture data assimilation. One of the motivations of this
113 study is to evaluate the skill improvement of soil moisture estimates through the assimilation of these
114 two widely-used satellite retrievals, which are produced by different remote sensing technologies in
115 terms of radiation bands and active or passive sensors. A careful comparison of the data from the
116 observation data sensitivity experiments using identical LSM and the data assimilation technique will
117 help understand the relative advantages or disadvantages of the two satellite retrievals. Another
118 motivation of this study is to apply several metrics that measure the skill improvement in the satellite
119 soil moisture data assimilation in a quantitative manner. The skill improvement can be contributed by
120 many factors, such as the quality of the assimilated satellite retrievals (relative to the open loop
121 estimates), the number of remote-sensing data being assimilated, and the accuracy of the model
122 background. Often these impacts are entangled in the data assimilation system output and hardly
123 decomposed by conventional metrics. In this regard, there are insufficient studies in previous literature

124 that quantify the individual contribution of each factor to the skill increase. One goal of this study is to
125 help identify the dominant factors. This information can eventually be utilized for planning future soil
126 moisture remote sensing technologies.

127 In this study, we carry out a series of soil moisture data assimilation experiments with active
128 and passive microwave retrievals designed to investigate the impact based on the following objectives.
129 The first objective is to investigate the skill improvement of surface and root-zone soil moisture through
130 the assimilation of SMAP and ASCAT soil moisture retrievals into the Joint U.K. Land Environment
131 Simulator (JULES) LSM using the Local Ensemble Transform Kalman Filter (LETKF), a variant of the
132 EnKF. Key distinguishing features of the LETKF are its efficiency of parallel computation through
133 separating the domain into independent local patches and that the LETKF enables to inflate the analysis
134 error covariance. Skill improvement relative to model-only (open loop) estimates is assessed versus in
135 situ soil moisture measurements. The second objective is to introduce assimilation metrics that break
136 down the skill improvement into three quantitative components: (i) the skill of the assimilated soil
137 moisture retrievals relative to open loop simulation, (ii) an approximation of the Kalman gain, and (iii)
138 the number of assimilated observations. Finally, following previous studies that demonstrated the value
139 of satellite soil moisture assimilation to enhance the drought monitoring (Mladenova et al., 2019; Xu et
140 al., 2020), we assess the benefit of assimilating satellite soil moisture retrievals in the context of drought
141 monitoring, specifically its potential for the U.S. drought monitoring system
142 (<https://droughtmonitor.unl.edu/>).

143 The paper is organized as follows. Section 2 introduces the model and datasets used in this
144 study. Section 3 describes the assimilation methodology, our validation approach, and the assimilation
145 metrics. Section 4 presents and discusses the results of this study. Finally, Section 5 summarizes the
146 results and their implications for future studies.

147

148 **2. Model and Data**

2.1 JULES Land Surface Model

This study uses the JULES community LSM (Best et al., 2011) developed by the U. K. Met Office. The soil moisture sub-model consists of 4 vertical layers of 0.1, 0.25, 0.65, and 2 meters in thickness. In this study, the model is set up with a 50 km spatial resolution. Land cover classes in JULES consist of five plant functional types (broadleaf trees, needleleaf trees, C3 temperate grass, C4 tropical grass, and shrubs) and four non-vegetation types (urban, inland water, bare soil, and land-ice). Surface parameters (e.g., albedo, roughness length) are specified for each land cover, and the model prognostic variables (e.g., soil moisture) are determined in response to atmospheric forcing variables, including 2-m air temperature and humidity, precipitation, 10-m wind speed, radiative fluxes, and pressure at the surface. In this study, the surface meteorological forcing variables except precipitation are obtained from the 6-hourly, 55-year Japanese Reanalysis (JRA-55) with 0.56° spatial resolution (Kobayashi et al., 2015). The forcing dataset is linearly interpolated to the model spatial resolution. Precipitation forcing, which is the most critical input determining soil moisture accuracy in land surface modeling, uses the Global Satellite Mapping of Precipitation (GSMaP; Aonashi et al., 2009; Kubota et al., 2007; Ushio et al., 2003; Ushio et al., 2009). GSMaP originally provides an hourly, gauge-calibrated rain rate with a 10 km spatial resolution over a quasi-global domain (60°S – 60°N). This study uses the GSMaP precipitation data within the 60°S – 60°N latitude band and JRA-55 for the rest of the model domain. GSMaP has been processed to the 6-hourly averaged data to match the temporal resolution of the JRA-55 reanalysis.

Errors in the JULES model estimates are propagated through an ensemble approach. Following Reichle et al., (2008), selected surface meteorological forcing variables and model prognostic variables are perturbed with random numbers, specifically radiation, rainfall, and soil moisture. As displayed in Table 1, normally distributed, additive perturbations are used for the 0-10 cm (top) layer soil moisture prognostic variable and the longwave radiation forcing, while lognormally distributed multiplicative perturbation are used for the precipitation and shortwave radiation forcing. The ensemble mean of additive and multiplicative perturbations is 0 and 1, respectively. All random perturbations are subject

175 to a first-order autoregressive (AR1) process with correlation time scales of 1 day for forcing variables
 176 and 3 hours for soil moisture content. Moreover, perturbations are also correlated spatially with a
 177 correlation scale of 50 km following an isotropic exponential decay model. In addition, cross-
 178 correlations, imposed on perturbations of the precipitation and radiation fields, ensure physical
 179 consistency between the meteorological forcing variables. For example, a positive perturbation of the
 180 downward shortwave radiation is (statistically) paired with a negative perturbation of the downward
 181 longwave radiation and precipitation. A detailed description of perturbing the surface meteorological
 182 forcing and model prognostic variables is provided in Reichle et al., (2008).

183

184 **Table 1** Parameters for perturbations to near-surface atmospheric boundary forcing variables and
 185 JULES soil moisture model prognostic variable at 0-10 cm (top) layer. A first-order auto-regressive
 186 (AR1) model is used for temporal correlations. Spatial correlation lengths scales are isotropic.

Perturbation variables	Additive (A) / Multiplicative (M)	Standard deviation	AR1 correlation time scale	Spatial correlation
Precipitation	M	0.5	1 day	50 km
Downward shortwave (SW)	M	0.3	1 day	50 km
Downward longwave (LW)	A	50 W m ⁻²	1 day	50 km
Soil moisture content	A	0.002 m ³ m ⁻³	3 hours	50 km

187

188 **2.2 Data**

189 2.2.1 In situ soil moisture measurements

190 For the validation, this study uses in situ soil moisture measurements from the U.S. Natural

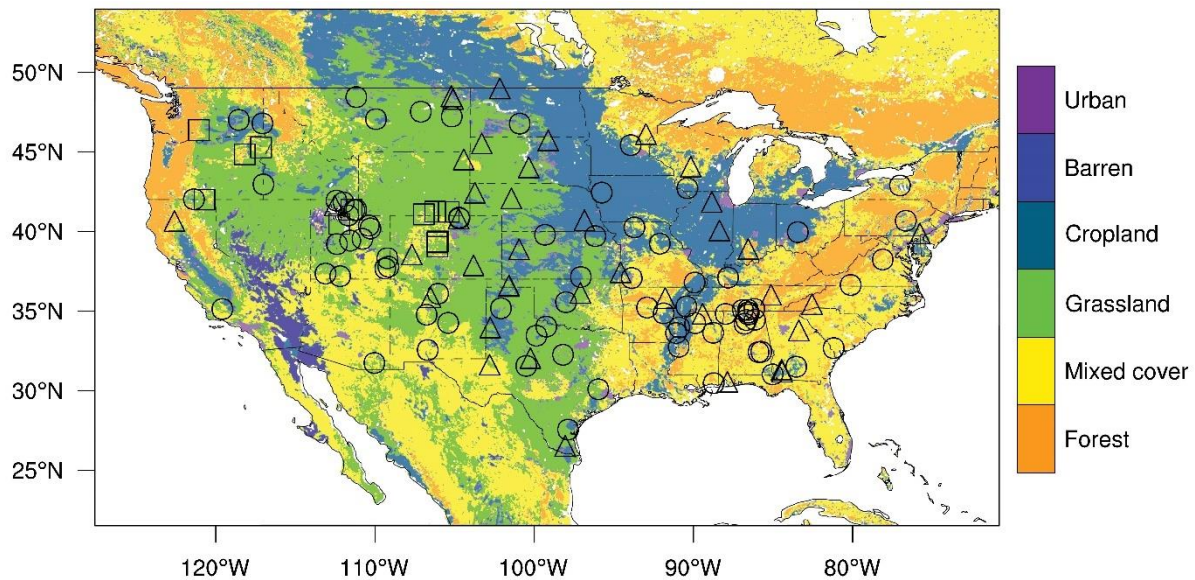
191 Resources Conservation Service (NRCS) Soil Climate Analysis Network (SCAN; Schaefer et al., 2007),
192 the U.S. Climate Reference Network (USCRN; Diamond et al., 2013; Bell et al., 2013), and the
193 Snowpack Telemetry (SNOTEL) network. Data are provided as hourly measurements at 5, 10, and 20
194 cm depths with flags for problematic observations in terms of data quality. Only datasets of “good”
195 quality and simultaneously measured at three different depths are used. We further discard unrealistic
196 values such as the data beyond the physically possible range and exclude measurements when the soil
197 is frozen. After the quality control of the hourly data, we calculate daily mean soil moisture.

198 Two additional screens are imposed before a measurement site is used in the validation of the
199 assimilation estimates. First, sites must have the data available more than 50 % during the entire
200 validation period. Second, sites with the particularly poor skill of either the SMAP or ASCAT satellite
201 retrievals relative to the open loop estimates ($R_{sat} - R_{openloop} < -0.2$) are excluded. This criterion
202 screens out 109 in situ measurement stations out of 244, and the remaining 135 stations are used for the
203 validation. This second screen avoids validation at sites where the satellite data should not be
204 assimilated in the first place, leaving the enhancement of the QC algorithm for future work. The network
205 sites used in the validation of the data assimilation results are mapped in Figure 1. Finally, in situ
206 “surface” soil moisture corresponds to measurements at 5 cm depth, and in situ “root-zone” soil
207 moisture corresponds to a layer thickness-weighted average of the measurements at 5, 10, and 20 cm
208 depths.

209 Validation results are broken down by land cover type (Figure 1). Land cover is from the
210 MODIS Collection 5 product (Friedl et al., 2010), which provides data at 500 m spatial resolution with
211 17 International Geosphere-Biosphere Programme (IGBP) classifications (Loveland and Belward 1997):
212 (1) evergreen needleleaf forests, (2) evergreen broadleaf forests, (3) deciduous broadleaf forests, (4)
213 deciduous needleleaf forests, (5) mixed forests, (6) closed shrubland, (7) open shrublands, (8) woody
214 savannas, (9) savannas, (10) grasslands, (11) permanent wetlands, (12) croplands, (13) urban and built-
215 up lands, (14) cropland/natural vegetation mosaics, (15) permanent snow and ice, (16) barren, and (17)
216 water. For the analysis by land cover, we grouped IGBP classes 6-9 and 14 into a broader “mixed land

217 cover” class. The validation is performed at the point of in situ observations in which 0.5 deg modeled
218 soil moisture estimates are interpolated. If the point of in situ sites is on a specified land cover, we
219 define the result over there.

220



221

222 **Figure 1** Location of monitoring sites of the SCAN (circle), USCRN (triangle), and SNOTEL
223 (square) networks over the continental U.S. Overlaid are the MODIS land cover classes with “forest”
224 consisting of IGBP classes 1-5 and “mixed cover” consisting of IGBP classes 6-9 and 14.

225

226 2.2.2 Assimilated satellite soil moisture retrievals

227 This study assimilates near-surface soil moisture datasets provided by the L-band (1.4 GHz)
228 passive (radiometer) microwave SMAP Level-2 product (O’Neill et al., 2019) and the C-band (5.3 GHz)
229 active (radar) microwave ASCAT product
230 (<https://navigator.eumetsat.int/product/EO:EUM:DAT:METOP:SOMO25>). The SMAP and ASCAT
231 data are available from May 2015 and from October 2006 to the present, respectively. As mentioned
232 above, the spatial resolution and soil penetration depth differ for the two datasets. Moreover, the SMAP
233 retrievals, unlike the ASCAT retrievals, are subject to errors in their ancillary inputs of soil temperature

234 and vegetation water content (Paloscia and Pampaloni 1988; Schmugge et al., 1986). In contrast, the
235 ASCAT data are more sensitive to noise from multiple scattering, especially over topographically
236 complex, wetland, and forest regimes (Dobson and Ulaby 1986).

237 The observation error standard deviations in the data assimilation are set to $0.04 \text{ m}^3 \text{ m}^{-3}$ for
238 SMAP retrievals (Chan et al., 2016) and 10% (in relative saturation units) for ASCAT retrievals (Dorigo
239 et al., 2010). In both cases, spatially and temporally constant values are used. Prior to assimilation,
240 quality control for the satellite data is applied based on the data quality flags provided with each satellite
241 dataset. Additionally, observations are discarded where MODIS land cover indicates forests ($> 60\%$
242 trees and woody vegetation) or grid cells with a wetland cover area fraction greater than 10% (indicated
243 by ASCAT data). The ASCAT data are also discarded, where topographical complexity exceeds 10%
244 (Draper et al., 2012). Finally, we exclude soil moisture retrievals from the assimilation whenever the
245 modeled surface temperature is less than 274 K, precipitation exceeds 50 mm day^{-1} , or the land is
246 covered by snow in the model simulation.

247

248 **3. Methodology**

249 **3.1 Data assimilation method**

250 The assimilation is performed using the LETKF (Hunt et al., 2007; Miyoshi and Yamane 2007).
251 Similar to the EnKF used in the SMAP L4_SM algorithm (Reichle et al., 2017b), the LETKF scheme
252 used here separates the domain into a number of independently processed local patches. When analyzing
253 the model states at the center of each local patch, all nearby observations within the local patch are used,
254 which allows for efficient parallel computations in a spatially distributed analysis. Unlike the EnKF of
255 the L4_SM algorithm, the LETKF used here is a deterministic filter that does not perturb the assimilated
256 observations, thereby avoiding the concomitant sampling noise.

257 In the following, X denotes the state vector within a specified local patch, and subscripts b and
258 a denote the prior (i.e., background) and the updated (i.e., analysis) states, respectively. The dimension

259 of X is $L \times N$ composed of an L dimensional local patch of N ensemble members. Generally, the local
 260 patch could be 3-dimensional, characterized by horizontal and vertical grid extent. However, this study
 261 defines only a 2-dimensional, horizontal local patch (150 km \times 150 km) because only top layer soil
 262 moisture is analyzed. Formally, the analyzed state vector X_a is given by

$$263 \quad X_a = \bar{X}_a + \delta X_a \quad (1)$$

264 where \bar{X}_a is an $L \times 1$ matrix of analysis ensemble means and δX_a denotes an $L \times N$ matrix of analysis
 265 perturbations. They are defined by

$$266 \quad \bar{X}_a = \bar{x}_b + \delta \tilde{x}_a \quad (2)$$

$$267 \quad \delta \tilde{x}_a = \delta X_b \tilde{P}_a (\delta Y)^T R^{-1} d \quad (3)$$

268 In Eq. (2), \bar{x}_b indicates the background forecast mean and $\delta \tilde{x}_a$ denotes the analysis increment. In Eq.
 269 (3), δX_b , \tilde{P}_a , δY , R , and d are background forecast perturbation, analysis error covariance, forward
 270 operated forecast ensemble perturbations, observation error covariance, and observational innovation,
 271 respectively. The observational innovation vector d is the difference between observations y_0 and their
 272 background ensemble mean counterparts $\overline{H(X_b)}$, where H is possibly a nonlinear observation operator
 273 and is replaced with the linearized version. The observation operator projects the modeled soil moisture
 274 background to the locations of the satellite observations using bilinear interpolation.

275 The forward-operated background forecast ensemble and the analysis error covariance in
 276 observation space are written as

$$277 \quad \delta Y = H(X_b) \quad (4)$$

$$278 \quad \tilde{P}_a = [\delta Y^T R^{-1} \delta Y + (N - 1)I/\rho]^{-1} \quad (5)$$

279 where ρ is a covariance inflation parameter for the analysis error covariance. The parameter ρ helps
 280 avoid the underestimation of the covariance which is a common problem of filter divergence caused by
 281 the assumption of spatially and temporally constant forcing and observation errors and the use of a
 282 limited number of ensemble members. In this study, we apply a multiplicative covariance inflation of

283 20 % of the spread (i.e., $\rho = 1.2$). After calculating analysis ensemble states for all independent local
284 patches, we collect the analysis results from each local patch into analysis for the entire domain.

285 Covariance localization is a useful method to moderate spurious sample error correlation
286 estimates by applying a distance-dependent reduction of the sample error covariance estimates (Hamill
287 et al., 2001; Houtekamer and Mitchell 2001). The LETKF scheme contains the weighting function of
288 the localization by separation into local patches. The function weights 1 inside and 0 outside the local
289 patch and by weighting the observational error covariance according to the distance from the local patch
290 center (Hunt et al., 2007). The covariance localization via the weighting function within the local patch
291 works by assigning larger errors to more distant observations (Miyoshi and Yamane 2007). The more
292 closely the weighting function of the covariance localization is centered around the local patch center,
293 the more the scheme resembles a 1-D filter. It can be realized by multiplying the observation error
294 covariance by the inverse of the smooth weighting function within each local patch in which the range
295 of weighting function is possibly 0 to 1. The weighting function $w(r_i)$ is based on a Gaussian function
296 as

$$297 \quad w(r_i) = \exp(-r_i^2/2\sigma^2) \quad (6)$$

298 where r_i denotes the distance of i -th observation within each local patch from the local patch center and
299 σ represents a localization scale parameter. In this experiment, we use a localization length scale
300 parameter value of 30 km. That is, the LETKF is set up almost like a 1-D filter, with weights of just
301 $10^{-2} \sim 10^{-3}$ near the edge of the local patch.

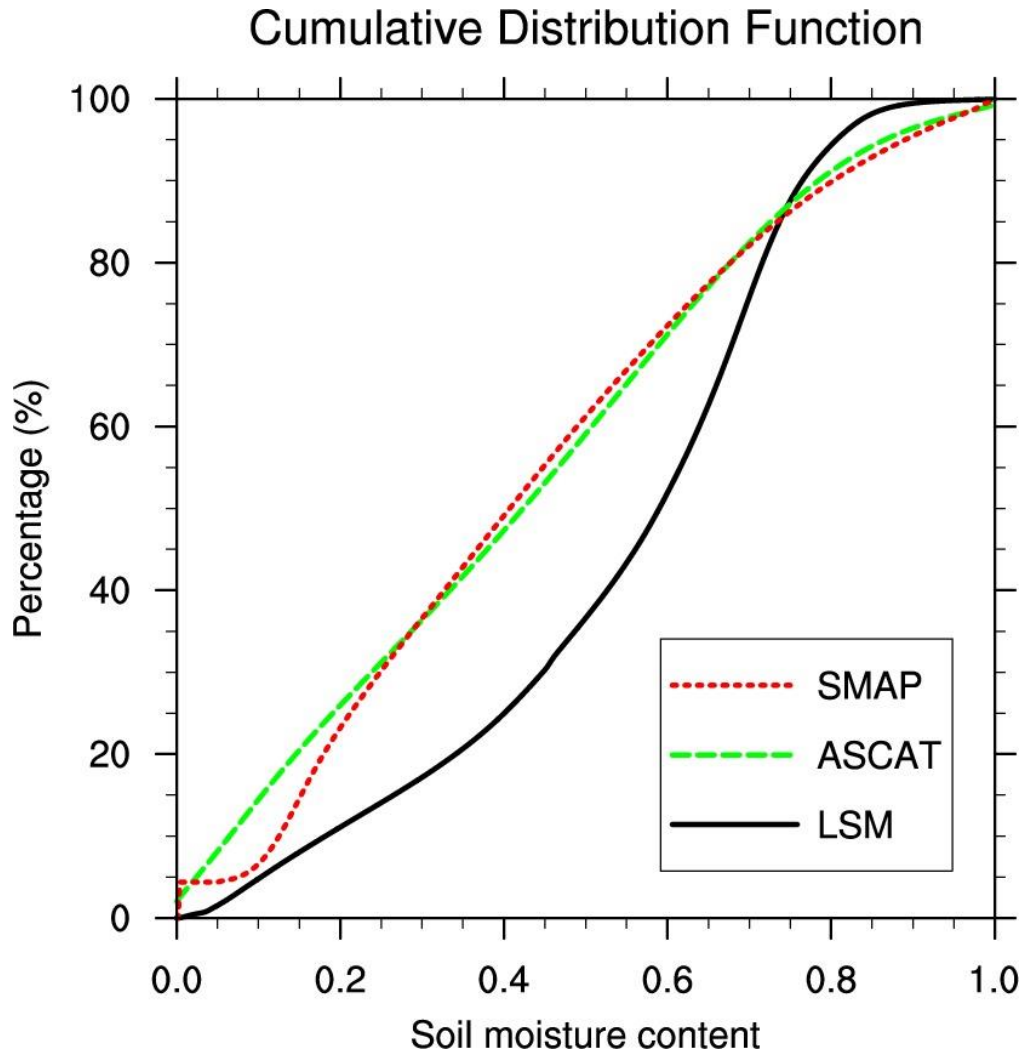
302

303 **3.2 Bias correction**

304 There is often a large discrepancy between soil moisture contents from remote sensing
305 retrievals and LSMs, owing to uncertainties in model physics and forcing data and differences in the
306 associated layer depths. These discrepancies manifest in sometimes large biases in the mean, variance,
307 and higher-moment statistics of soil moisture between the satellite retrievals and the model simulation.

308 One way to correct for such biases is to match the cumulative distribution functions (CDFs) between
309 the satellite dataset and the model simulation (Reichle and Koster 2004). Such a CDF matching adjusts
310 all moments and differs from a linear rescaling that matches only the mean values and standard
311 deviations based on the assumption of a Gaussian distribution (Yilmaz and Crow 2013). CDF matching,
312 which is used here, is thus more appropriate for representing skewed datasets and also avoids violating
313 the variables' physical bounds. Over North America, for instance, the CDFs of surface soil moisture
314 from SMAP retrievals, ASCAT retrievals, and the LSM open loop simulation differ considerably (Fig.
315 2). Prior to data assimilation, the raw SMAP and ASCAT soil moisture retrievals are rescaled to the
316 LSM climatology based on the CDFs, which is done separately for each grid cell. The specified
317 observation error standard deviation is also rescaled using the ratio of the standard deviation of the
318 satellite to modeled soil moisture time series at each grid cell (Liu et al., 2011).

319



320

321 **Figure 2** The cumulative distribution function of surface soil moisture content as a fraction of
 322 saturation from SMAP retrievals (April 2015–December 2019), ASCAT retrievals (January 2010–
 323 December 2019), and the LSM open loop simulation (January 2010–December 2019) over North
 324 America (130°W–75°W, 30°N–50°N).

325

326 **3.3 Data assimilation experiments**

327 This study performs three data assimilation experiments by specifying different sets of soil
 328 moisture retrieval data to be assimilated into the JULES LSM, including two single-sensor experiments
 329 using SMAP and ASCAT satellite retrievals, respectively, and a combined SMAP plus ASCAT multi-
 330 sensor experiment, hereafter referred to as DA(SMAP), DA(ASCAT), and DA(SMAP+ASCAT),

331 respectively. The specific description of the LSM configuration and data assimilation method was
332 provided in Sections 2.1 and 3.1, respectively. The experiments use 12 ensemble member and a 3-hour
333 assimilation cycle. They are conducted for May-September of 2015–2019. As a baseline, a 12-member,
334 open loop ensemble experiment is also performed using the same ensemble perturbations but no data
335 assimilation. The open loop skill serves as a baseline for measuring the skill improvement from the
336 satellite data assimilation.

337

338 **3.4 Validation strategy**

339 The assimilation and open loop estimates are validated against the in situ soil moisture
340 measurements described in Section 2.2.1. This study primarily measures the skill in temporal variations
341 using the Pearson correlation coefficient (R) applied to anomaly time series, calculated by removing
342 monthly-mean values for each calendar month. This anomaly correlation is computed for daily averages
343 of the surface and root-zone anomaly soil moisture. This study also measures the data assimilation
344 performance based on the unbiased root-mean-square error (ubRMSE) of the raw soil moisture time
345 series (Entekhabi et al., 2010b), which avoids some of the shortcomings of the RMSE metric in the
346 presence of mean bias. Based on the Fisher Z transform, we compute approximate 95% confidence
347 levels for the anomaly correlations at in situ sites. These confidence levels depend on the estimated R
348 value and the number of degrees of freedom. The 95% confidence intervals are calculated by averaging
349 the 95% confidence intervals across the in situ sites and subsequently dividing by the square root of the
350 number of sites. The model surface soil moisture is validated against in situ measurements at 5 cm depth,
351 and the model root-zone soil moisture is validated against the depth-weighted root-zone in situ
352 measurements defined in Section 2.2.1. The skill improvement of the data assimilation with respect to
353 the open loop is defined as the R value of the assimilated product minus that of the open loop model.

354

355 **3.5 Assimilation metrics**

356 This study introduces quantitative assimilation metrics to decompose skill improvement from
 357 data assimilation. Three components determine the impact of the data assimilation on the model
 358 estimates: (1) the skill difference between the satellite retrievals and the open loop estimates (ΔR_{sat}),
 359 (2) the approximate weighting of the assimilated observations in the analysis update (KG), and (3) the
 360 average number of assimilated observation samples (N_{sat}). Each metric is written as

$$361 \quad \Delta R_{sat} = R_{sat} - R_{openloop} \quad (7)$$

$$362 \quad KG = \sum_{t=1}^{N_{days}} \left[\frac{E_b(t)}{E_b(t)+E_o(t)} \right] / N_{days} \quad (8)$$

$$363 \quad N_{sat} = \sum_{t=1}^{N_{days}} \sum_{i=1}^n w(r_i)_t / N_{days} \quad (9)$$

364 In Eq. (7), R_{sat} is the temporal anomaly correlation (Section 3.4) between remotely sensed retrievals
 365 (y_0) and the in situ surface soil moisture observations. Similarly, $R_{openloop}$ is the temporal anomaly
 366 correlation between the open loop surface soil moisture and the in situ measurements. In Eq. (8), $E_b(t)$
 367 and $E_o(t)$ are the error variances of the model background and the observation of surface soil moisture
 368 at each analysis time, respectively, and N_{days} denotes the number of days over the entire assimilation
 369 period. By construction, the value of KG is bounded between 0 and 1. High values of KG imply that the
 370 analysis of soil moisture is closer to the observation than to the background. Note that KG is a rough
 371 approximation of the diagonal element of the Kalman gain matrix in the LETKF scheme. In Eq. (9), the
 372 number of assimilated observation samples is defined as the time average of the sum of the localization
 373 weights (i.e., Eq. (6)) within the local patch at each analysis time.

374

375 **3.6 Soil moisture condition index**

376 This study also applies the assimilated soil moisture information to drought monitoring using
 377 the soil moisture condition index (SMCI) introduced in Zhang and Jia (2013). This index uses weekly-
 378 mean values and is designed to capture the development of short-term dryness. The index should be

379 comparable across regions, regardless of the background climatology, and does not reflect seasonality.
380 It is written as

$$381 \quad SMCI = \frac{SM - SM_{min}}{SM_{max} - SM_{min}} \quad (10)$$

382 where SM represents a weekly-averaged surface soil moisture, and the subscripts max and min
383 indicate the maximum and the minimum values for each corresponding week at each grid cell from the
384 71 years (1948–2018) long-term JULES offline simulation. The first 62 years (1948–2009) of the LSM
385 offline simulation are forced with surface meteorological data from Sheffield et al., (2006), and the rest
386 of the period (2010–2018) is from the LSM run driven by the JRA-55 reanalysis corrected with the 6-
387 hourly GSMaP rainfall. The index is bounded between 0 to 1. At a given grid cell, the closer the drought
388 index is to zero, the more severe the drought.

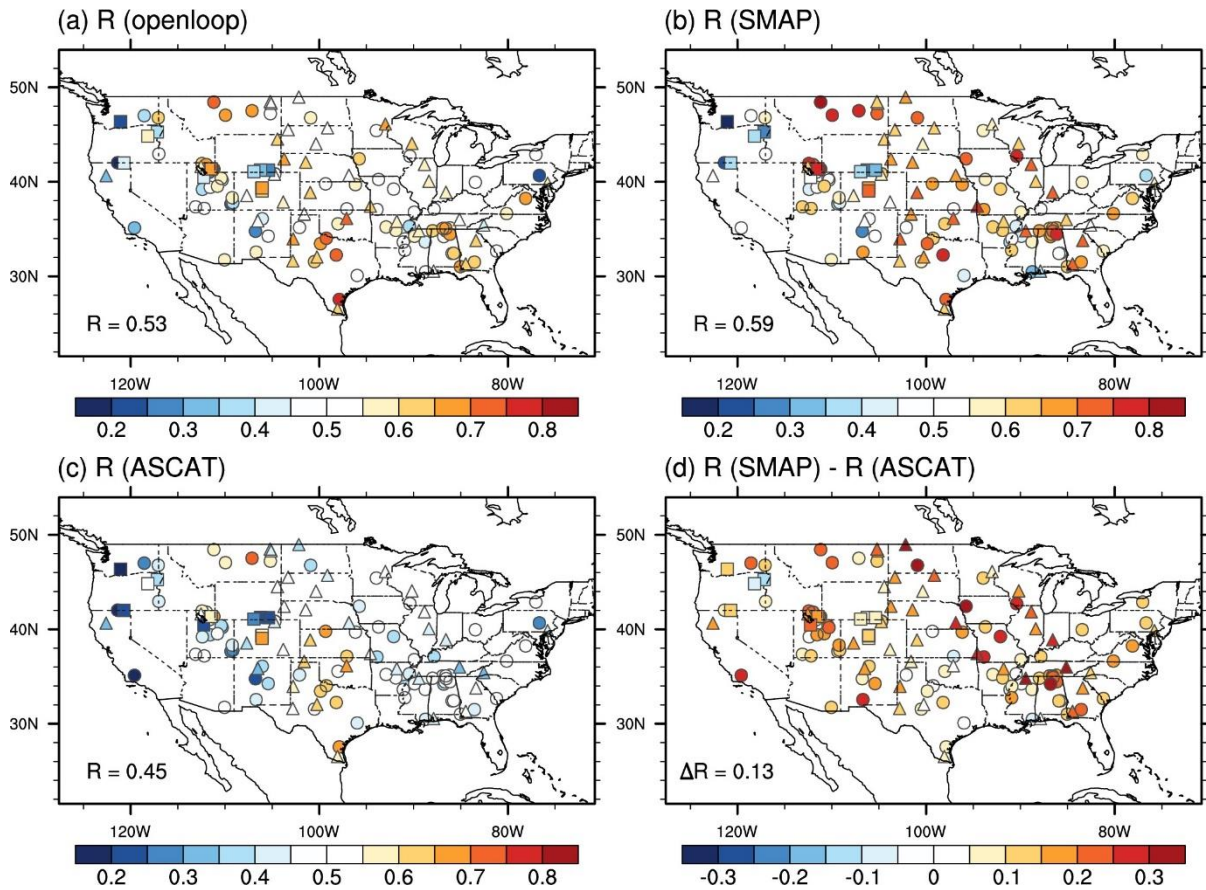
389

390 **4. Results**

391 **4.1 Skill of satellite and open loop soil moisture estimates**

392 Before we investigate the results of the soil moisture assimilation, we examine the skill of the
393 satellite and open loop estimates. Figure 3 shows the anomaly correlation coefficient for the open loop
394 (Fig. 3a), the SMAP retrievals (Fig. 3b), and the ASCAT retrievals (Fig. 3c) against in situ
395 measurements in the continental U.S. The average R values of the open loop, SMAP retrievals, and
396 ASCAT retrievals are 0.53, 0.59, and 0.45, respectively. The skill of SMAP is best overall and clearly
397 better than that of ASCAT ($\Delta R \sim 0.13$) over the entire U.S. without any obvious regional pattern (Fig.
398 3d).

399



400

401 **Figure 3** Surface soil moisture skill measured as the anomaly correlation coefficient R with the in
 402 situ measurements from (a) the open loop model, (b) SMAP retrievals, and (c) ASCAT retrievals. (d)
 403 shows the skill difference between SMAP and ASCAT retrievals, with red (blue) colors indicating that
 404 SMAP retrievals have higher (lower) skill than ASCAT retrievals.

405

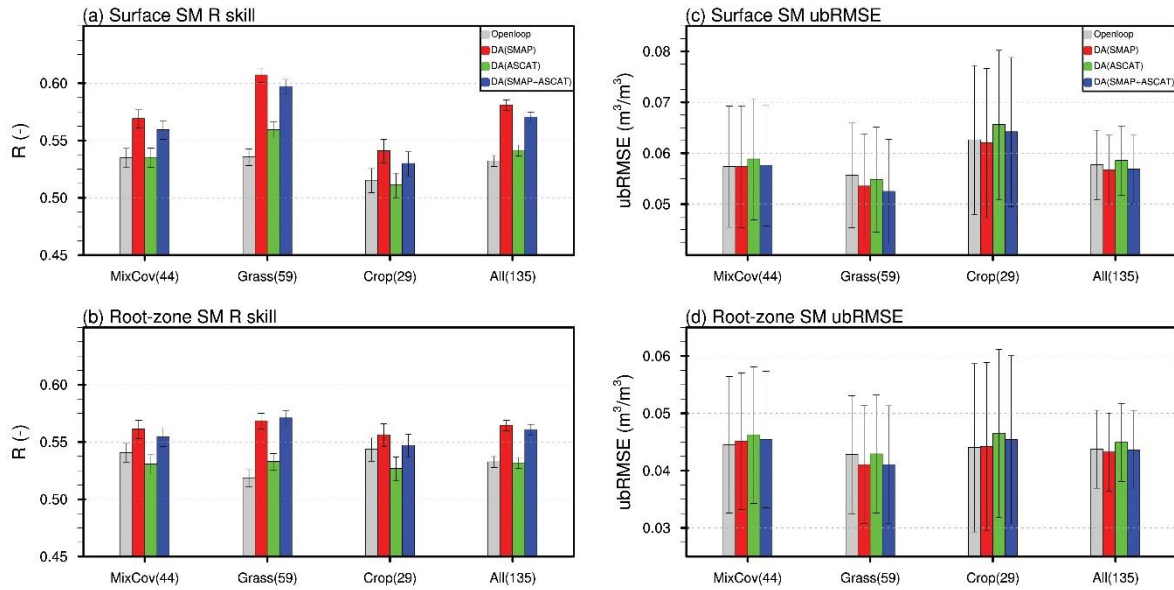
406 4.2 Skill of soil moisture estimates from data assimilation experiments

407 Figure 4 compares the average skill of surface and root-zone soil moisture estimates from the open
 408 loop with the three experiments that assimilate (i) SMAP retrievals only, (ii) ASCAT retrievals only,
 409 and (iii) both SMAP and ASCAT retrievals. The average anomaly correlation skill of surface soil
 410 moisture (Fig. 4a) is increased in the assimilation experiments by 0.05 (DA(SMAP)), 0.01
 411 (DA(ASCAT)), and 0.04 (DA(SMAP+ASCAT)), respectively, compared to the open loop ($R=0.53$),
 412 which represents a statistically significant improvement (at the 5% significance level) when SMAP data

413 are included in the assimilation. The relative performance is similar when measured with the ubRMSE,
414 although the ubRMSE reductions are not statistically significant (Fig. 4c). The skill improvement is
415 greater for grasslands than for the other land cover classes, which will be discussed further in the next
416 sub-section. The result implies that the satellite retrievals provide added value through data assimilation.
417 Even though ASCAT observations are additionally assimilated in DA(SMAP+ASCAT) compared to
418 DA(SMAP), the skill of DA(SMAP+ASCAT) is slightly worse than that of DA(SMAP), which suggests
419 that the assimilation system is less optimal for DA(SMAP+ASCAT) than for DA(SMAP). Some sub-
420 optimality is unavoidable because the satellite observations are assimilated into a non-linear model
421 (here, JULES LSM) and the errors are never entirely Gaussian and uncorrelated. This suggests that
422 there is little added benefit from assimilating the ASCAT retrievals, which have relatively poor skill
423 compared to the SMAP retrievals and the open loop run (Fig. 3).

424 Although only surface soil moisture observations are assimilated, there is also an indirect positive
425 impact on sub-surface (root-zone) soil moisture (Fig. 4b). The anomaly correlation of root-zone soil
426 moisture is increased in the assimilation experiments by 0.04 (DA(SMAP) and DA(SMAP+ASCAT)),
427 compared to the open loop ($R=0.53$), but the skill improvements in the root-zone are not as large as
428 those in the surface. In particular, the assimilation of SMAP retrievals results in a significant
429 improvement of the root-zone soil moisture skill (except for crops), while the impact of the ASCAT
430 assimilation on the root-zone skill is neutral on average. The neutral impact of the ASCAT assimilation
431 on the root-zone soil moisture skill is expected because only the surface soil moisture states are updated
432 directly in our analysis and the skill improvement in the surface soil moisture in DA(ASCAT) is
433 marginal (Fig. 4a). The relative performance is again similar when measured with the ubRMSE,
434 although the ubRMSE reductions are again not statistically significant (Fig. 4d). Finally, we obtained
435 similar results for the surface and root-zone validation when using only days and locations for which
436 satellite observations were assimilated (not shown).

437

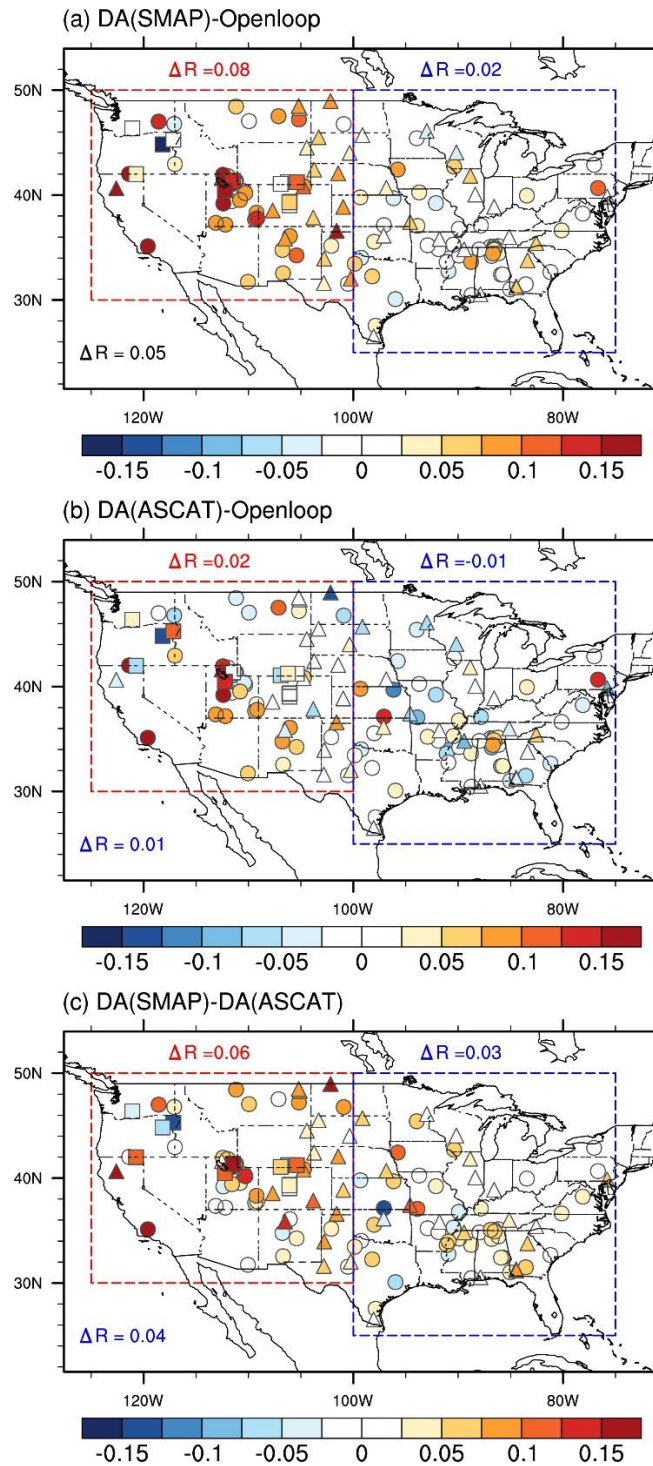


438

439 **Figure 4** (a, b) R skill and (c, d) ubRMSE of (a, c) surface and (b, d) root-zone soil moisture
 440 estimates from the open loop (gray), DA(SMAP) (red), DA(ASCAT) (green), and DA(SMAP+ASCAT)
 441 (blue). The soil moisture estimates are validated against in situ measurements over North America (see
 442 Fig. 1 for locations) and averaged for each land cover class. Error bars represent 95% confidence
 443 intervals.

444

445 The skill of soil moisture estimates from all assimilation experiments is commonly increased, but
 446 the magnitude of the improvements depends on the data source and the region. Figures 5a and 5b show
 447 the spatial distributions of the skill improvement from the open loop by DA(SMAP) and DA(ASCAT)
 448 experiments, respectively. Both experiments generally show improved performance, especially in the
 449 western U.S., even though the skill increase is less pronounced in DA(ASCAT). The larger
 450 improvement in the western U.S. is consistent with the clear performance improvement over grasslands
 451 (i.e., Fig. 4), as most of the western U.S. is classified as grasslands. Figure 5c compares the skill
 452 difference between DA(SMAP) and DA(ASCAT) (Fig. 5c). When the regions are separated into the
 453 western (125°W–100°W, 25°N–50°N) and the eastern U.S. (100°W–70°W, 25°N–50°N), the
 454 improvements from DA(SMAP) exceed those from DA(ASCAT) by $\Delta R \sim 0.06$ over the western U.S.
 455 and by $\Delta R \sim 0.03$ over the eastern U.S.. This result is further investigated in the following sub-section.



457

458 **Figure 5** Skill difference between surface soil moisture estimates from (a) DA(SMAP) and the
 459 open loop, (b) DA(ASCAT) and the open loop, and (c) DA(SMAP) and DA(ASCAT). The bottom-left
 460 value in each panel is averaged across the entire domain. The red and blue dashed boxes indicate the

461 western and eastern U.S., respectively, and the value above the box represents the average of the values
462 in each box.

463

464 **4.3 Component analysis for the skill improvement**

465 In an effort to better understand the differences in the skill improvements among the soil moisture
466 data assimilation experiments, this section examines the assimilation metrics introduced in Section 3.5.
467 Specifically, this section further examines the following three key points: (i) the skill of DA(SMAP) is
468 higher than DA(ASCAT), (ii) the two single-sensor assimilation experiments concurrently reveal the
469 higher skill improvement in the western U.S. compared to the eastern U.S., and (iii) the skill difference
470 in both single-sensor experiments is higher in the western U.S. compared to the eastern U.S..

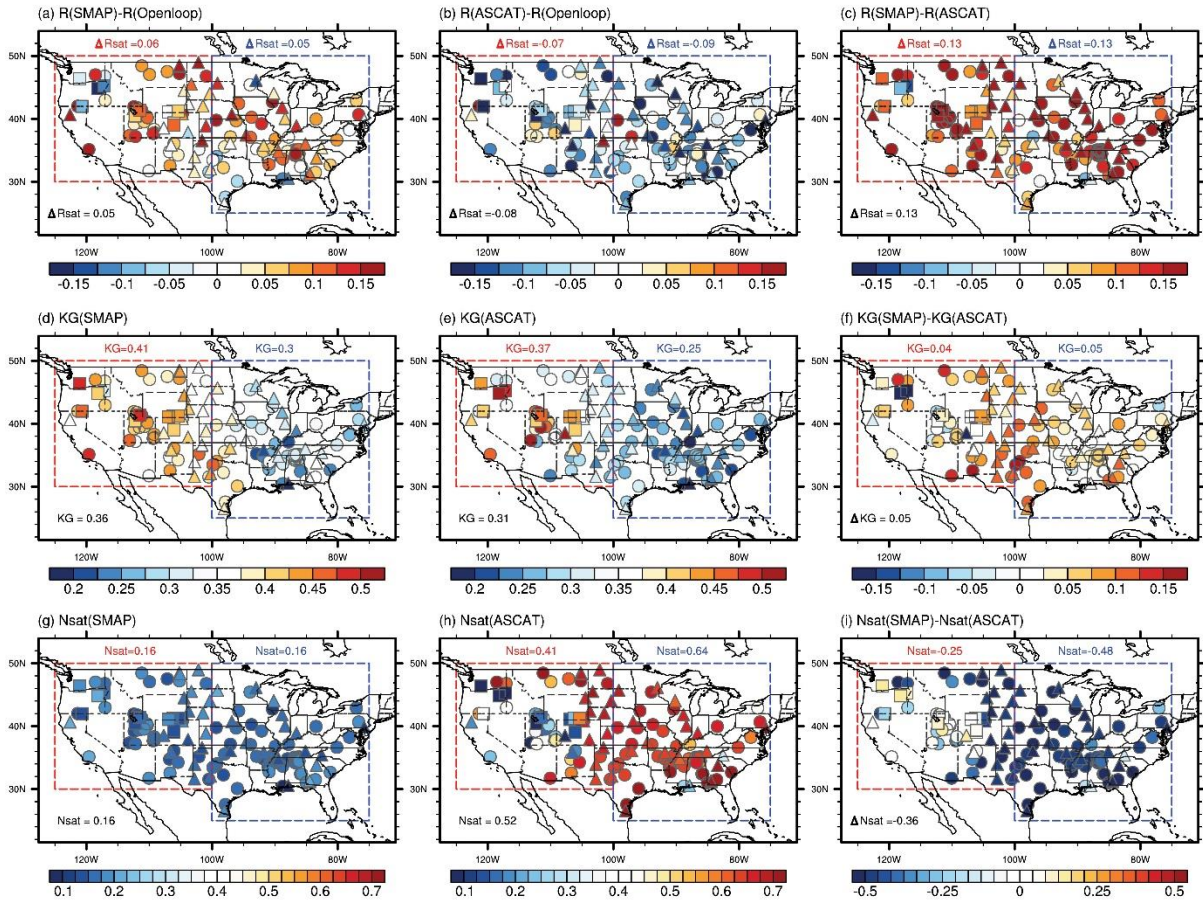
471 Figures 6 represents the spatial distributions of the assimilation metrics for the two single sensor
472 assimilation experiments and their difference. The average ΔR_{sat} from SMAP is greater than that of
473 ASCAT over the continental U.S. (Figs. 6a and 6b), mostly due to the higher skill of SMAP compared
474 to ASCAT retrievals as indicated in Fig. 3d. The significantly better quality of the SMAP retrievals
475 makes a clear difference in the results of the data assimilation (c.f., Fig. 5c).

476 Furthermore, KG values from the DA(SMAP) and DA(ASCAT) experiments are higher in the
477 western than the eastern U.S. (Figs. 6d and 6e), which is mostly attributed to the spatial distribution of
478 the model background error (E_b) rather than that of observation error (E_o) (not shown). Therefore, KG
479 contributes to the improvement in the performance of data assimilation particularly in the western U.S.
480 in both single-sensor assimilation experiments (c.f., Figs. 5a and 5b). Lastly, in trying to identify which
481 factor plays a dominant role in the regional dependence of the skill improvement in the two single-
482 sensor experiments (Fig. 5c), we note that the ΔR_{sat} values for SMAP and ASCAT are similar for the
483 western and eastern U.S. (Figs. 6c). This similarity for the western and eastern U.S. also applies to the
484 KG difference values between DA(SMAP) and DA(ASCAT) (Fig. 6f). On the other hand, the
485 corresponding N_{sat} difference values are quite different for the western and eastern U.S. (Fig. 6i). This

486 west-east discrepancy primarily originates with the N_{sat} values for DA(ASCAT) (Fig. 6h) because
487 there is little west-east discrepancy in DA(SMAP) (Fig. 6g).

488 Note also that the number of assimilated observations within each local patch is considerably
489 smaller in DA(SMAP) than in DA(ASCAT) (compare Fig. 6g and 6h). For instance, the N_{sat} values
490 for DA(SMAP) and DA(ASCAT) over the Continental U.S. are 0.16 and 0.52, respectively (Figs. 6g
491 and 6h). First, ASCAT has finer spatial resolution than SMAP. Second, DA(ASCAT) utilizes two
492 satellite sensors (METOP-A and METOP-B) in complementary orbits, instead of just one for
493 DA(SMAP). Even accounting for the fact that ASCAT retrievals are from two satellite sensors (i.e.,
494 $N_{sat} = \sim 0.3$ for each of the two sensors), the ASCAT N_{sat} value is still nearly two times larger than
495 that of SMAP, which can be explained by the difference in spatial resolution between SMAP and
496 ASCAT. Additionally, the number of assimilated ASCAT observations in the eastern U.S. is larger than
497 that in the western U.S., which is due to the quality control of the retrievals. For instance, ASCAT
498 observations are discarded when the topographic complexity flag provided with the retrievals is larger
499 than 10%. The mountainous terrain of the western U.S. thus leads to a decrease in N_{sat} for DA(ASCAT).
500 When the quality control process for the ASCAT observations with topographic complexity is omitted
501 in a separate, one-year (2016) experiment, the soil moisture assimilation skill drops by $\Delta R = -0.01$.
502 Consequently, the skill values of the DA(SMAP) and DA(ASCAT) experiments are more different in
503 the western U.S., because a relatively smaller number of ASCAT observations is assimilated there.

504



505

506

507

508

509

510

511

512

513

514

515

Figure 6 The spatial distribution of (a, b) the skill difference between the satellite retrievals and the open loop (ΔR_{sat}), (d, e) the approximate Kalman gain (KG), and (g, h) the effective number of assimilated observational samples (N_{sat}). The results are from (a, d, and g) DA(SMAP) and (b, e, and h) DA(ASCAT). Panels (c, f, and i) in the last column show, separately for each row, the difference between the results for the two experiments. The bottom-left value in each panel represents the average across the entire domain. The red and blue dashed boxes indicate the western and eastern U.S., respectively, and the value above each box represents the average of the values within each box. The number of sites in the western and the eastern sub-domain is 69 and 66, respectively.

4.4 Validation of the drought event

516

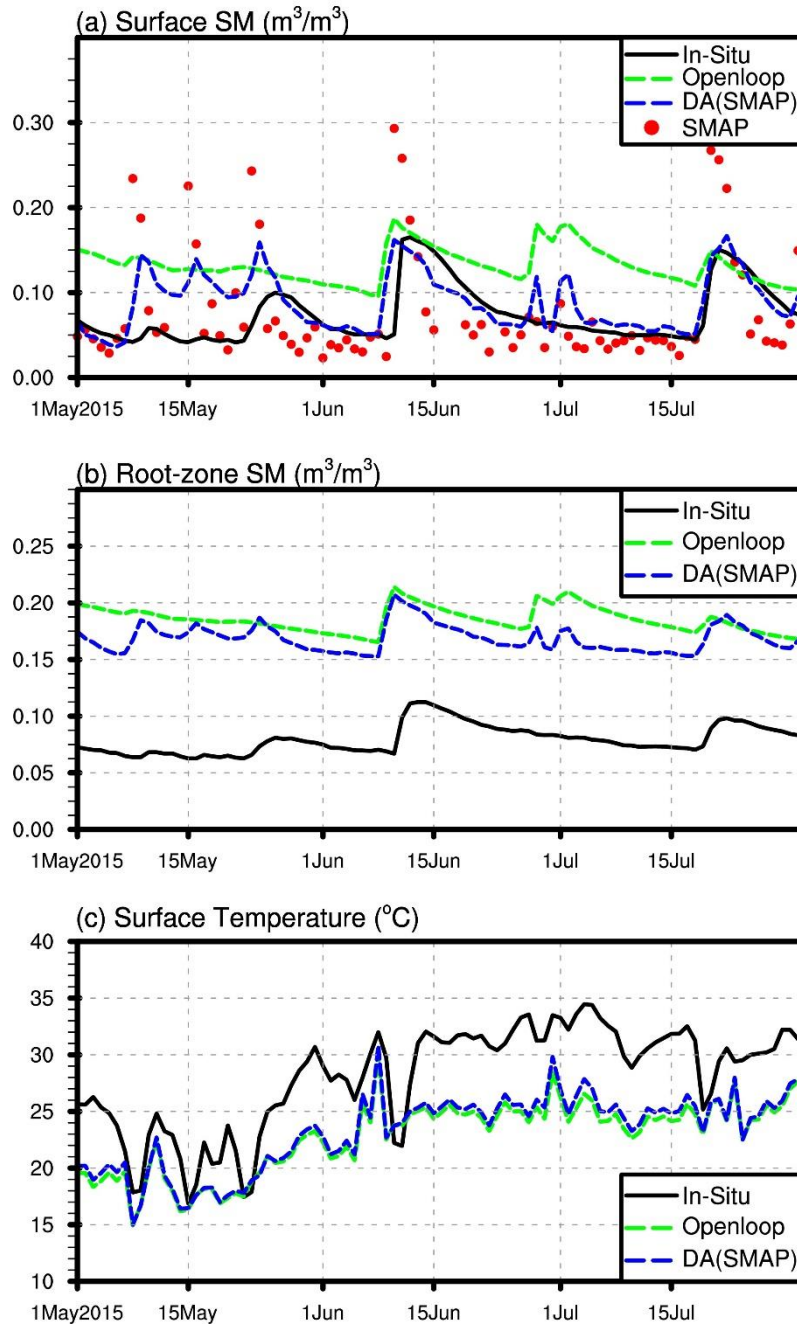
517

There were several drought events since 2015 over the western U.S., especially in California. This section investigates the impact of soil moisture assimilation on the representation of hydrological

518 climate extremes such as a severe drought. Hereafter the soil moisture estimates from DA(SMAP) are
519 presented as the best performance results. Figure 7 represents the daily time series of soil moisture and
520 temperature from in situ observations, the open loop simulation, and DA(SMAP) at Cochora Ranch
521 station in California during May-July 2015. DA(SMAP) clearly captures the dry surface and root-zone
522 soil moisture conditions much better than the open loop simulation, even though the improvement is
523 not always prominent due to the absence of satellite observations such as in mid-May when the SMAP
524 retrieval is sampled much less. At this location, the RMSE of the surface (root-zone) soil moisture is
525 reduced from $0.068 \text{ m}^3 \text{ m}^{-3}$ ($0.107 \text{ m}^3 \text{ m}^{-3}$) for the open loop model to $0.035 \text{ m}^3 \text{ m}^{-3}$ ($0.090 \text{ m}^3 \text{ m}^{-3}$) for
526 the SMAP assimilation for May–July 2015. The drier soil moisture conditions in the assimilation
527 experiment lead to the surface flux partitioning away from latent heat flux and toward increased sensible
528 heat flux, which finally reduces the cold bias in the experiment. As a result, there is a slight improvement
529 from the assimilation in the simulation of surface temperature.

530

Cochora Ranch (SCAN)



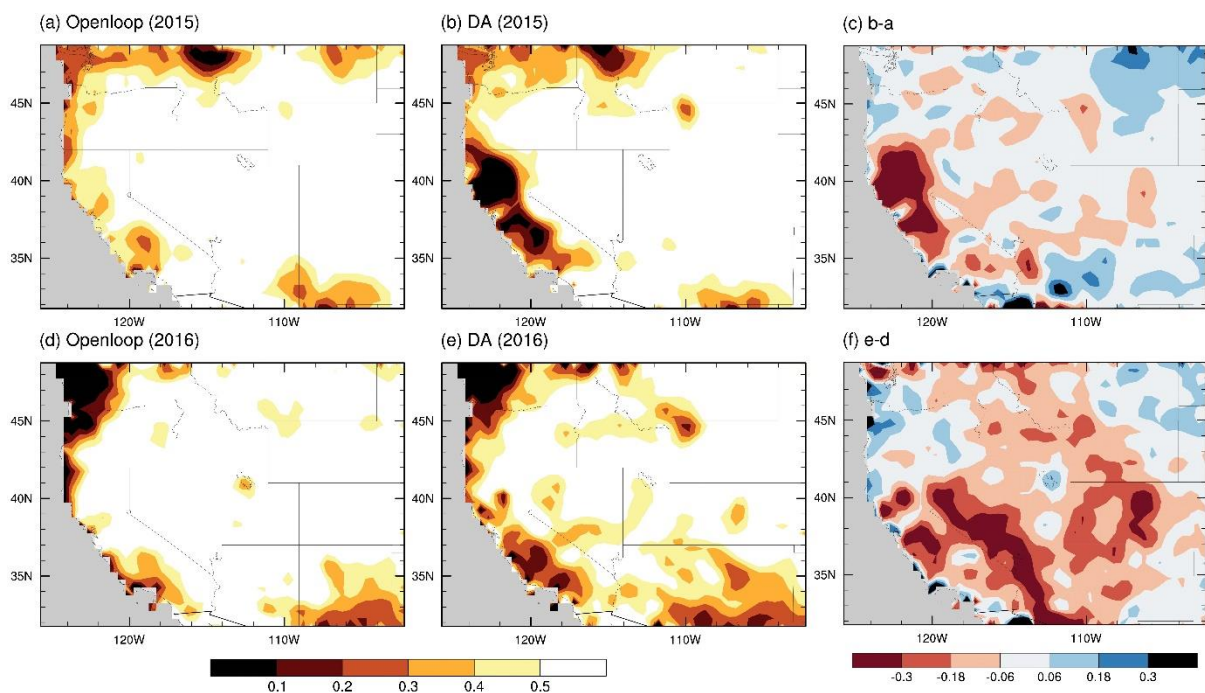
531

532 **Figure 7** Time series of (a) surface soil moisture, (b) root-zone soil moisture, and (c) land surface
533 temperature at Cochora Ranch station (35.12°N , 119.6°W) in California from in situ measurements
534 (black lines), DA(SMAP) (blue lines), the open loop model (green lines), and the SMAP retrievals (red
535 dots).

536

537 Furthermore, the soil moisture assimilation estimates constrained by the SMAP satellite retrievals
 538 provide a more realistic spatial representation of drought conditions. The western U.S. suffered extreme
 539 drought from 2015 to 2016, with the most severe impacts seen in California (Supplementary Figures 1
 540 and 2, respectively). Figure 8 represents the spatial patterns of the SMCI drought index based on surface
 541 soil moisture estimates. The figure shows that the spatial distribution of land surface dryness in the
 542 western U.S. is better represented by DA(SMAP) than in the open loop simulation. The drought index
 543 from the satellite assimilation for 2 years reveals more similar features to the U.S. drought monitoring
 544 information presented in the Supplementary Figures compared with the result of the open loop,
 545 especially in California, where the most severe drought occurred. The drought assessment only based
 546 on the assimilated soil moisture estimate shows the spatial distribution of the land surface dryness. In
 547 contrast, it is not consistent with the coherent dry conditions from the U.S. drought monitoring system
 548 based on various variables such as precipitation, surface temperature, streamflow, and so on, as well as
 549 soil moisture contents without any assimilation.

550



551

552 **Figure 8** Weekly SMCI drought index for 5 May–2 June 2015 (top row) and 3 May–31 May 2016
 553 (bottom row) from the open loop model (left column) and DA(SMAP) (middle column). The SMCI

554 difference between DA(SMAP) and the open loop is shown in the right column.

555

556 **5. Conclusion**

557 This study develops a data assimilation system based on the JULES land surface model and the
558 LETKF scheme. The system assimilates soil moisture retrievals from L-band passive (SMAP) and C-
559 band active (ASCAT) microwave remote sensing observations. The retrievals are subject to quality
560 control and, prior to the data assimilation, are rescaled into the model soil moisture climatology using
561 CDF fitting. Based on this data assimilation framework, we examine the impact of remote sensing
562 retrievals on the assimilated soil moisture estimates through validation with ground-based
563 measurements. This study investigates three different soil moisture assimilation experiments with the
564 LETKF scheme: (i) single-sensor assimilation of SMAP retrievals, (ii) single-sensor assimilation of
565 ASCAT retrievals, and (iii) combined assimilation of SMAP and ASCAT retrievals. The results reveal
566 that both sets of satellite retrievals provide added value in the representation of surface and root-zone
567 soil moisture in the assimilation estimates over the continental U.S. The skill improvement is more
568 pronounced in the relatively dry grasslands regions of the western U.S. The result from the SMAP
569 assimilation experiment shows the best performance, with surface and root-zone soil moisture skill
570 improvements of 0.05 and 0.03, respectively. On the other hand, the skill of the combined SMAP and
571 ASCAT assimilation estimates is similar to that of the SMAP-only assimilation, suggesting that the
572 assimilation of additional observations has little impact if they are of relatively lower quality.

573 The skill improvement of soil moisture estimates from the assimilation experiments can be broken
574 into three different components. The three assimilation metrics are (i) the relative skill of satellite
575 retrievals compared to that of the open loop, (ii) an approximation of the Kalman gain, and (iii) the
576 number of assimilated observations. Based on this diagnostic, the skill of soil moisture estimates from
577 the SMAP assimilation over the continental US is higher than that from the ASCAT assimilation mainly
578 owing to the better quality of the SMAP retrievals. It is also found that the higher skill improvement in
579 the western compared to the eastern U.S. is explained by the Kalman gain in both DA(SMAP) and

580 DA(ASCAT). Moreover, the skill difference between two single-sensor assimilation experiments
581 shows a large regional dependence. Specifically, the SMAP assimilation estimates show relatively
582 higher skill compared to the ASCAT assimilation estimates in the western U.S. than in the eastern U.S..
583 This result is attributed mainly to the fact that relatively fewer ASCAT observations are assimilated in
584 the western U.S.. During quality control, ASCAT retrievals are discarded when the topographical
585 complexity index exceeds 10 %. Even though there are smaller west-east differences in the relative skill
586 of satellite retrievals and the Kalman gain between both experiments, the difference in the number of
587 assimilated data contributes dominantly to the larger skill difference in the western U.S..

588 Finally, the assessment of drought conditions is enhanced through the assimilation of SMAP soil
589 moisture retrievals. The soil moisture assimilation estimates better match the observed extremely dry
590 conditions for the 2015 and 2016 western U.S. drought events. This finding corroborates the emerging
591 use of SMAP soil moisture estimates in the U.S. Drought Monitor and suggests that soil moisture
592 estimates from an advanced land data assimilation system that ingests SMAP and other satellite
593 observations may further improve the current drought monitoring.

594 Looking further ahead, improved soil moisture estimates from the land data assimilation system
595 developed in this study may also improve the initialization of dynamical forecast models. As the soil
596 moisture strongly controls the energy and water balance at the land surface interface, this approach
597 should lead to a better prediction of the atmospheric states through the realistic representation of land-
598 atmosphere interaction. This is especially true in regions with scarce precipitation observations (e.g.,
599 much of South America, Africa, Asia, and Australia) where the performance of soil moisture estimates
600 from open loop simulations is less reliable.

601

602 **Acknowledgments**

603 This study was supported by the Korea Meteorological Administration Research and
604 Development Program under Grant KMI2018-03110. Rolf Reichle was supported by the
605 NASA SMAP mission and the NASA SMAP Science Team.

- Al-Yaari, A., Wigneron, J.-P., Dorigo, W., Colliander, A., Pellarin, T., Hahn, S., Mialon, A., Richaume, P., Fernandez-Moran, R., & Fan, L. (2019). Assessment and inter-comparison of recently developed/reprocessed microwave satellite soil moisture products using ISMN ground-based measurements. *Remote Sensing of Environment*, *224*, 289-303
- Albergel, C., De Rosnay, P., Gruhier, C., Muñoz-Sabater, J., Hasenauer, S., Isaksen, L., Kerr, Y., & Wagner, W. (2012). Evaluation of remotely sensed and modelled soil moisture products using global ground-based in situ observations. *Remote Sensing of Environment*, *118*, 215-226
- Aonashi, K., Awaka, J., Hirose, M., Kozu, T., Kubota, T., Liu, G., Shige, S., Kida, S., Seto, S., & Takahashi, N. (2009). GSMaP passive microwave precipitation retrieval algorithm: Algorithm description and validation. *Journal of the Meteorological Society of Japan. Ser. II*, *87*, 119-136
- Bateni, S., & Entekhabi, D. (2012). Relative efficiency of land surface energy balance components. *Water resources research*, *48*
- Bell, J.E., Palecki, M.A., Baker, C.B., Collins, W.G., Lawrimore, J.H., Leeper, R.D., Hall, M.E., Kochendorfer, J., Meyers, T.P., & Wilson, T. (2013). US Climate Reference Network soil moisture and temperature observations. *Journal of hydrometeorology*, *14*, 977-988
- Best, M., Pryor, M., Clark, D., Rooney, G., Essery, R., Ménard, C., Edwards, J., Hendry, M., Porson, A., & Gedney, N. (2011). The Joint UK Land Environment Simulator (JULES), model description–Part 1: energy and water fluxes. *Geoscientific Model Development*, *4*, 677-699
- Chan, S.K., Bindlish, R., O'Neill, P.E., Njoku, E., Jackson, T., Colliander, A., Chen, F., Burgin, M., Dunbar, S., & Piepmeier, J. (2016). Assessment of the SMAP passive soil moisture product. *IEEE Transactions on Geoscience and Remote Sensing*, *54*, 4994-5007
- De Jeu, R.A. (2003). Retrieval of land surface parameters using passive microwave remote sensing. *PhD diss., Vrije Universiteit Amsterdam*
- De Lannoy, G., & Reichle, R. (2016). Assimilation of SMOS brightness temperatures or soil moisture retrievals into a land surface model. *Hydrology and Earth System Sciences*, *20*, 4895-4911
- De Lannoy, G.J., Reichle, R.H., Houser, P.R., Arsenault, K.R., Verhoest, N.E., & Pauwels, V.R. (2010). Satellite-scale snow water equivalent assimilation into a high-resolution land surface model. *Journal of hydrometeorology*, *11*, 352-369
- De Rosnay, P., Drusch, M., Vasiljevic, D., Balsamo, G., Albergel, C., & Isaksen, L. (2013). A simplified Extended Kalman Filter for the global operational soil moisture analysis at ECMWF. *Quarterly Journal of the Royal Meteorological Society*, *139*, 1199-1213
- Diamond, H.J., Karl, T.R., Palecki, M.A., Baker, C.B., Bell, J.E., Leeper, R.D., Easterling, D.R., Lawrimore, J.H., Meyers, T.P., & Helfert, M.R. (2013). US Climate Reference Network after one decade of operations: Status and assessment. *Bulletin of the American Meteorological Society*, *94*, 485-498
- Dirmeyer, P.A., Jin, Y., Singh, B., & Yan, X. (2013). Trends in land–atmosphere interactions from CMIP5 simulations. *Journal of hydrometeorology*, *14*, 829-849
- Dobson, M.C., & Ulaby, F.T. (1986). Active microwave soil moisture research. *IEEE Transactions on*

Geoscience and Remote Sensing, 23-36

Dorigo, W., Scipal, K., Parinussa, R.M., Liu, Y.Y., Wagner, W., De Jeu, R.A., & Naeimi, V. (2010). Error characterisation of global active and passive microwave soil moisture data sets

Draper, C., Reichle, R., De Lannoy, G., & Liu, Q. (2012). Assimilation of passive and active microwave soil moisture retrievals. *Geophysical Research Letters*, 39

Entekhabi, D., Njoku, E.G., O'Neill, P.E., Kellogg, K.H., Crow, W.T., Edelstein, W.N., Entin, J.K., Goodman, S.D., Jackson, T.J., & Johnson, J. (2010a). The soil moisture active passive (SMAP) mission. *Proceedings of the IEEE*, 98, 704-716

Entekhabi, D., Reichle, R.H., Koster, R.D., & Crow, W.T. (2010b). Performance metrics for soil moisture retrievals and application requirements. *Journal of hydrometeorology*, 11, 832-840

Forman, B.A., Reichle, R., & Rodell, M. (2012). Assimilation of terrestrial water storage from GRACE in a snow-dominated basin. *Water resources research*, 48

Friedl, M.A., Sulla-Menashe, D., Tan, B., Schneider, A., Ramankutty, N., Sibley, A., & Huang, X. (2010). MODIS Collection 5 global land cover: Algorithm refinements and characterization of new datasets. *Remote Sensing of Environment*, 114, 168-182

Gao, H., Wood, E.F., Jackson, T., Drusch, M., & Bindlish, R. (2006). Using TRMM/TMI to retrieve surface soil moisture over the southern United States from 1998 to 2002. *Journal of hydrometeorology*, 7, 23-38

Hamill, T.M., Whitaker, J.S., & Snyder, C. (2001). Distance-dependent filtering of background error covariance estimates in an ensemble Kalman filter. *Monthly Weather Review*, 129, 2776-2790

Houtekamer, P.L., & Mitchell, H.L. (2001). A sequential ensemble Kalman filter for atmospheric data assimilation. *Monthly Weather Review*, 129, 123-137

Hunt, B.R., Kostelich, E.J., & Szunyogh, I. (2007). Efficient data assimilation for spatiotemporal chaos: A local ensemble transform Kalman filter. *Physica D: Nonlinear Phenomena*, 230, 112-126

Kerr, Y.H., Waldteufel, P., Wigneron, J.-P., Delwart, S., Cabot, F., Boutin, J., Escorihuela, M.-J., Font, J., Reul, N., & Gruhier, C. (2010). The SMOS mission: New tool for monitoring key elements of the global water cycle. *Proceedings of the IEEE*, 98, 666-687

Kobayashi, S., Ota, Y., Harada, Y., Ebata, A., Moriya, M., Onoda, H., Onogi, K., Kamahori, H., Kobayashi, C., & Endo, H. (2015). The JRA-55 reanalysis: General specifications and basic characteristics. *Journal of the Meteorological Society of Japan. Ser. II*, 93, 5-48

Koster, R., Mahanama, S., Yamada, T., Balsamo, G., Berg, A., Boisserie, M., Dirmeyer, P., Doblas-Reyes, F., Drewitt, G., & Gordon, C. (2011). The second phase of the global land-atmosphere coupling experiment: soil moisture contributions to subseasonal forecast skill. *Journal of hydrometeorology*, 12, 805-822

Kubota, T., Shige, S., Hashizume, H., Aonashi, K., Takahashi, N., Seto, S., Hirose, M., Takayabu, Y.N., Ushio, T., & Nakagawa, K. (2007). Global precipitation map using satellite-borne microwave radiometers by the GSMaP project: Production and validation. *IEEE Transactions on Geoscience and Remote Sensing*, 45, 2259-2275

Lahoz, W.A., & De Lannoy, G.J. (2014). Closing the gaps in our knowledge of the hydrological cycle

over land: Conceptual problems. *Surveys in Geophysics*, *35*, 623-660

Lievens, H., Reichle, R.H., Liu, Q., De Lannoy, G., Dunbar, R.S., Kim, S., Das, N.N., Cosh, M., Walker, J.P., & Wagner, W. (2017). Joint Sentinel-1 and SMAP data assimilation to improve soil moisture estimates. *Geophysical Research Letters*, *44*, 6145-6153

Liu, Q., Reichle, R.H., Bindlish, R., Cosh, M.H., Crow, W.T., de Jeu, R., De Lannoy, G.J., Huffman, G.J., & Jackson, T.J. (2011). The contributions of precipitation and soil moisture observations to the skill of soil moisture estimates in a land data assimilation system. *Journal of hydrometeorology*, *19*

Loveland, T.R., & Belward, A. (1997). The IGBP-DIS global 1km land cover data set, DISCover: first results. *International Journal of Remote Sensing*, *18*, 3289-3295

Miyoshi, T., & Yamane, S. (2007). Local ensemble transform Kalman filtering with an AGCM at a T159/L48 resolution. *Monthly Weather Review*, *135*, 3841-3861

Mladenova, I.E., Bolten, J.D., Crow, W.T., Sazib, N., Cosh, M.H., Tucker, C.J., & Reynolds, C. (2019). Evaluating the operational application of SMAP for global agricultural drought monitoring. *IEEE Journal of Selected Topics in Applied Earth Observations and Remote Sensing*, *12*, 3387-3397

Owe, M., de Jeu, R., & Holmes, T. (2008). Multisensor historical climatology of satellite-derived global land surface moisture. *Journal of Geophysical Research: Earth Surface*, *113*

Owe, M., de Jeu, R., & Walker, J. (2001). A methodology for surface soil moisture and vegetation optical depth retrieval using the microwave polarization difference index. *IEEE Transactions on Geoscience and Remote Sensing*, *39*, 1643-1654

Paloscia, S., & Pampaloni, P. (1988). Microwave polarization index for monitoring vegetation growth. *IEEE Transactions on Geoscience and Remote Sensing*, *26*, 617-621

Pan, M., Cai, X., Chaney, N.W., Entekhabi, D., & Wood, E.F. (2016). An initial assessment of SMAP soil moisture retrievals using high-resolution model simulations and in situ observations. *Geophysical Research Letters*, *43*, 9662-9668

Parinussa, R.M., Holmes, T.R., Wanders, N., Dorigo, W.A., & de Jeu, R.A. (2015). A preliminary study toward consistent soil moisture from AMSR2. *Journal of hydrometeorology*, *16*, 932-947

Reichle, R.H. (2008). Data assimilation methods in the Earth sciences. *Advances in Water Resources*, *31*, 1411-1418

Reichle, R.H., Crow, W.T., & Keppenne, C.L. (2008). An adaptive ensemble Kalman filter for soil moisture data assimilation. *Water resources research*, *44*

Reichle, R.H., De Lannoy, G.J., Liu, Q., Ardizzone, J.V., Colliander, A., Conaty, A., Crow, W., Jackson, T.J., Jones, L.A., & Kimball, J.S. (2017a). Assessment of the SMAP level-4 surface and root-zone soil moisture product using in situ measurements. *Journal of hydrometeorology*, *18*, 2621-2645

Reichle, R.H., De Lannoy, G.J., Liu, Q., Koster, R.D., Kimball, J.S., Crow, W.T., Ardizzone, J.V., Chakraborty, P., Collins, D.W., & Conaty, A.L. (2017b). Global assessment of the SMAP level-4 surface and root-zone soil moisture product using assimilation diagnostics. *Journal of hydrometeorology*, *18*, 3217-3237

Reichle, R.H., & Koster, R.D. (2004). Bias reduction in short records of satellite soil moisture. *Geophysical Research Letters*, *31*

- Reichle, R.H., Kumar, S.V., Mahanama, S.P., Koster, R.D., & Liu, Q. (2010). Assimilation of satellite-derived skin temperature observations into land surface models. *Journal of hydrometeorology*, *11*, 1103-1122
- Reichle, R.H., Liu, Q., Koster, R.D., Crow, W.T., De Lannoy, G.J., Kimball, J.S., Ardizzone, J.V., Bosch, D., Colliander, A., & Cosh, M. (2019). Version 4 of the SMAP Level-4 Soil Moisture Algorithm and Data Product. *Journal of Advances in Modeling Earth Systems*, *11*, 3106-3130
- Reichle, R.H., McLaughlin, D.B., & Entekhabi, D. (2001). Variational data assimilation of microwave radiobrightness observations for land surface hydrology applications. *IEEE Transactions on Geoscience and Remote Sensing*, *39*, 1708-1718
- Reichle, R.H., McLaughlin, D.B., & Entekhabi, D. (2002a). Hydrologic data assimilation with the ensemble Kalman filter. *Monthly Weather Review*, *130*, 103-114
- Reichle, R.H., Walker, J.P., Koster, R.D., & Houser, P.R. (2002b). Extended versus ensemble Kalman filtering for land data assimilation. *Journal of hydrometeorology*, *3*, 728-740
- Ridler, M.E., Madsen, H., Stisen, S., Bircher, S., & Fensholt, R. (2014). Assimilation of SMOS-derived soil moisture in a fully integrated hydrological and soil-vegetation-atmosphere transfer model in Western Denmark. *Water resources research*, *50*, 8962-8981
- Schaefer, G.L., Cosh, M.H., & Jackson, T.J. (2007). The USDA natural resources conservation service soil climate analysis network (SCAN). *Journal of Atmospheric and Oceanic Technology*, *24*, 2073-2077
- Schmugge, T., O'Neill, P.E., & Wang, J.R. (1986). Passive microwave soil moisture research. *IEEE Transactions on Geoscience and Remote Sensing*, 12-22
- Seneviratne, S.I., Corti, T., Davin, E.L., Hirschi, M., Jaeger, E.B., Lehner, I., Orlowsky, B., & Teuling, A.J. (2010). Investigating soil moisture–climate interactions in a changing climate: A review. *Earth-Science Reviews*, *99*, 125-161
- Seneviratne, S.I., Lüthi, D., Litschi, M., & Schär, C. (2006). Land–atmosphere coupling and climate change in Europe. *Nature*, *443*, 205-209
- Seo, E., Lee, M.-I., Jeong, J.-H., Koster, R.D., Schubert, S.D., Kim, H.-M., Kim, D., Kang, H.-S., Kim, H.-K., & MacLachlan, C. (2019). Impact of soil moisture initialization on boreal summer subseasonal forecasts: mid-latitude surface air temperature and heat wave events. *Climate dynamics*, *52*, 1695-1709
- Seo, E., Lee, M.-I., Schubert, S.D., Koster, R.D., & Kang, H.-S. (2020). Investigation of the 2016 Eurasia heat wave as an event of the recent warming. *Environmental Research Letters*, *15*, 114018
- Sheffield, J., Goteti, G., & Wood, E.F. (2006). Development of a 50-year high-resolution global dataset of meteorological forcings for land surface modeling. *Journal of Climate*, *19*, 3088-3111
- Torres, R., Snoeij, P., Geudtner, D., Bibby, D., Davidson, M., Attema, E., Potin, P., Rommen, B., Floury, N., & Brown, M. (2012). GMES Sentinel-1 mission. *Remote Sensing of Environment*, *120*, 9-24
- Ushio, T., Okamoto, K.i., Iguchi, T., Takahashi, N., Iwanami, K., Aonashi, K., Shige, S., Hashizume, H., Kubota, T., & Inoue, T. (2003). The global satellite mapping of precipitation (GSMaP) project. *Aqua (AMSR-E)*, 2004

- Ushio, T., Sasashige, K., Kubota, T., Shige, S., Okamoto, K.i., Aonashi, K., Inoue, T., Takahashi, N., Iguchi, T., & Kachi, M. (2009). A Kalman filter approach to the Global Satellite Mapping of Precipitation (GSMaP) from combined passive microwave and infrared radiometric data. *Journal of the Meteorological Society of Japan. Ser. II, 87*, 137-151
- Wagner, W., Hahn, S., Kidd, R., Melzer, T., Bartalis, Z., Hasenauer, S., Figa-Saldaña, J., de Rosnay, P., Jann, A., & Schneider, S. (2013). The ASCAT soil moisture product: A review of its specifications, validation results, and emerging applications. *Meteorologische Zeitschrift, 22*, 5-33
- Xu, L., Abbaszadeh, P., Moradkhani, H., Chen, N., & Zhang, X. (2020). Continental drought monitoring using satellite soil moisture, data assimilation and an integrated drought index. *Remote Sensing of Environment, 250*, 112028
- Yilmaz, M.T., & Crow, W.T. (2013). The optimality of potential rescaling approaches in land data assimilation. *Journal of hydrometeorology, 14*, 650-660
- Zhang, A., & Jia, G. (2013). Monitoring meteorological drought in semiarid regions using multi-sensor microwave remote sensing data. *Remote Sensing of Environment, 134*, 12-23